

Particle motion measurements near a rocky shore off Cabo Frio Island

S. M. Jesus,^{1,a)} F. C. Xavier,² R. P. Vio,² J. Osowsky,² M. V. S. Simões,² and E. B. F. Netto²

¹Laboratory of Robotics and Engineering Systems, University of Algarve, 8005-135 Faro, Portugal

²Instituto de Estudos do Mar Almirante Paulo Moreira, Brazilian Navy, Arraial do Cabo, Rio de Janeiro, Brazil

ABSTRACT:

This paper describes the lessons learned from the experiment BIOCOM'19 carried out in January 2019, in a shallow water bay off the island of Cabo Frio (RJ, Brazil). A dual accelerometer vector sensor hydrophone was deployed for two days, near a rocky shore covered with a significant benthic fauna. The results show that the frequency band above approximately 1.5 kHz is mostly associated with invertebrate biological noise and that the acoustic and the particle motion fields have a similar behavior, following the usual dawn-dusk activity pattern, and a coherent directivity content. At low frequencies, below ~300 Hz, the acoustic pressure and the particle acceleration fields have significantly different spectral content along time. Many of these differences are due to anthropogenic noise sources related with nearby boating activity, while during quiet periods, they may be attributed to the biological activity from the rocky shore. © 2020 Acoustical Society of America. <https://doi.org/10.1121/10.0001392>

(Received 19 December 2019; revised 26 May 2020; accepted 26 May 2020; published online 18 June 2020)

[Editor: Arthur N. Popper]

Pages: 4009–4019

I. INTRODUCTION

The interest on sound for monitoring and determining the impact of anthropogenic noise on marine life has received recent considerable and still increasing attention from the scientific community.^{1,2} This has naturally lead to the separate characterization of spatial and temporal distribution of anthropogenic noise in one hand, and biological related sound on the other hand. The characterization of biological sound is a complex task due to a number of factors among which are (i) the variety of sound-producing species leading to a wide range of sound levels, frequency bands, duration, repetition rates, etc.; (ii) sound superposition, making it difficult to isolate per species characteristic sound;³ and (iii) the variety of habitat and ecosystems, resulting in the generation and propagation of sound modulated by environmental factors that mask biological related features.⁴ In order to overcome some of these difficulties, several authors concentrated on the study of individual animals in tank controlled studies, which are extremely valuable for the understanding of the sound production and hearing mechanism.^{5,6} However, the characterization of individual animals does not always give us clues about the behavior of communities, an understanding of which is still lacking.

Passive acoustics is the natural approach for non-intrusive free-leaving biological sound communities' characterization but is impaired by the fact that many species do not produce sound but are sensitive to it. Further, it is now well known that some species are sensitive to acoustic pressure, some to acoustic particle motion, and some others to both.^{5,7,8} Early studies have reported important differences

between the acoustic pressure and the acoustic particle motion fields at low frequencies and raised concerns for its possible separate effects on fish with lateral line organs or other mechanoreceptors.⁹ Recently, several particle motion measurements were conducted during the installation¹⁰ and operation of wind turbines and the potential impact on fish.¹¹ The hearing mechanism of fish and invertebrates has been abundantly studied in the literature and, more recently, the often underestimated sensitivity to particle motion.^{8,12} Therefore, the motivation for performing particle motion measurements during the BIOCOM'19 sea trial was two-fold: (a) to determine differences between the acoustic pressure and the particle motion fields both in time and space, attempting to separate anthropogenic noise, such as that due to recreational boating and coastal sightseeing, and that biological related and (b) to compare acoustic pressure and particle motion biological signatures during anthropogenic noise free periods.

The BIOCOM'19 experiment took place in a protected bay close to the Island of Cabo Frio (23° S, 42° W), RJ, Brazil. In this area, the coast is characterized by rocky shores with an abundant coverage of crustaceans and invertebrates both aquatic or semi-aquatic, among which are shrimps, bivalves, barnacles, and sea urchins.¹³ In this region, there is a wide variety of fish, some of which are of relatively large size,¹⁴ possibly related to the nutrient rich upwelling regime occurring under propitious conjugation of NE wind and tide.¹⁵

The expected underwater chorus is therefore formed by the population of invertebrates on the rocky shore ecosystem strongly modulated by the tidal and upwelling regime, occasional fish, and, in the period of the year when the sea trial took place, strongly impacted by recreational boating noise

^{a)}Electronic mail: sjesus@ualg.pt

during the day time. The results uncovered in the present work correlate acoustic pressure and acoustic particle motion both in the biological band, above roughly 1.5 kHz, and differ in the low frequency band, below 300 Hz. This result is particularly significant for the directional data obtained from the vector sensor hydrophone, clearly identifying the separation between the anthropogenic and biological components.

This paper is organized as follows. Section II describes the material used and the methods implemented during the BIOCOM'19 experiment. Section III presents and discusses the results obtained. Section IV draws some conclusions and perspectives for further investigation.

II. MATERIAL AND METHODS

A. The experimental area

The BIOCOM'19 experiment took place in a protected bay in the Island of Cabo Frio, state of Rio de Janeiro, Brazil, from January 14 to 18, 2019 (Fig. 1). Please refer to Ref. 16 for an overview of the experiment objectives and details. This bay is fully open to the North East and through a narrow rocky 50m wide inlet, called Boqueirão, to the South West. Under propitious summer conditions of strong NE wind and rising tide, cold upwelling water seeps through the Boqueirão into the bay rapidly decreasing water temperature in the lower portion of the water column producing sometimes temperature shifts up to 10 °C. The annotated picture of Fig. 2 shows the location of the recording system (white X) close to the Boqueirão inlet, as well as the various possible source of environmental and anthropogenic noise present in the bay.¹⁷

B. Data recorders

The recording system installation is shown in the picture of Fig. 3(a) and is composed of a stainless steel quadrangular pyramid with the Dual Accelerometer Vector Sensor (DAVS) recorder on the top vertex (upright white cylinder with black end tip). Figure 3(b) is a drawing (not to

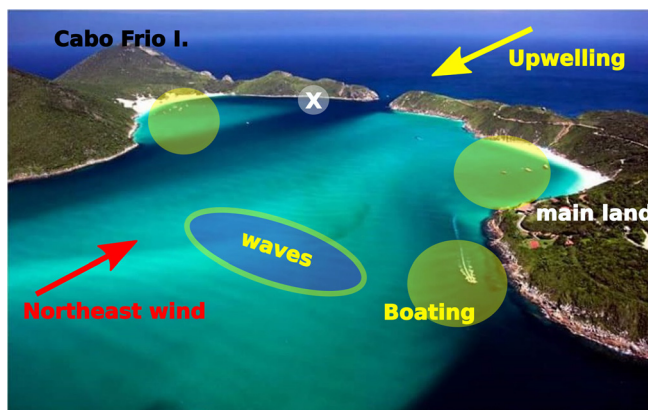


FIG. 2. (Color online) Cabo Frio Island bay (RJ, Brazil): sources of anthropogenic noise (boating-yellow circles) (Ref. 17) and environmental forcing (NE wind and upwelling). The recorder position is marked with a white X mark.

scale) that shows the approximate geometry of the experimental setup where the recorder is installed 1 m above the sea floor in approximately 8 m water depth and at 7 m straight from the island rocky shore that forms the inlet. As recorded during the experiment the tidal flow induces a water level variation of about 1 m. The horizontal distance at the surface between the rocky shore and the vertical to the recorder is about 25 m. The bottom at the recorder location is made of sand, at approximately 5 m of the base of the

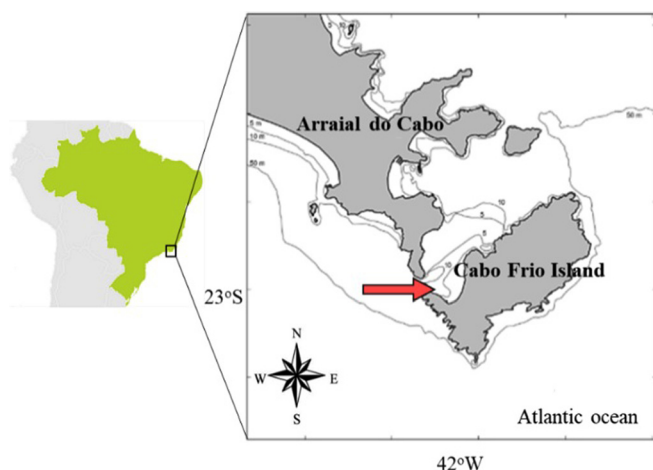
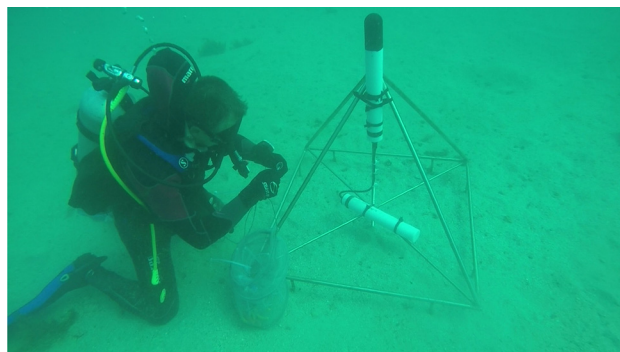
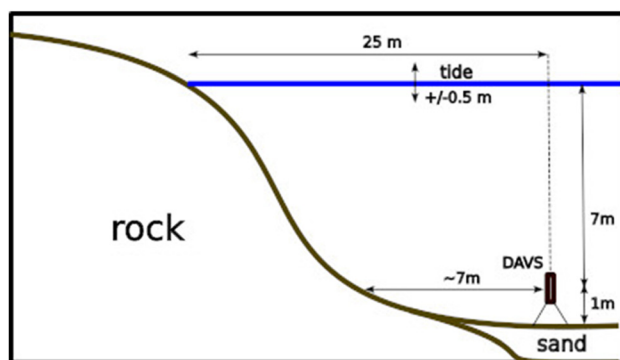


FIG. 1. (Color online) BIOCOM'19 experiment location at Cabo Frio Island bay (RJ, Brazil).

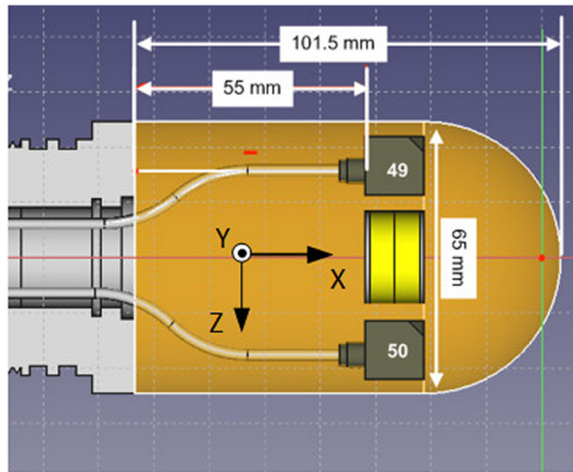


(a)

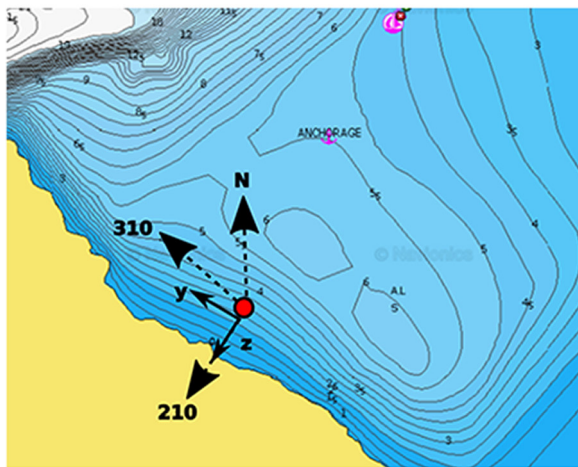


(b)

FIG. 3. (Color online) Bottom installation of the DAVS recorder (upright white cylinder with black tip) and the additional battery pack (underneath horizontal white cylinder) (a) and experimental setup geometry (b).



(a)



(b)

FIG. 4. (Color online) Drawing of DAVS sensing end, with positioning of accelerometers (black rectangles numbered 49 and 50) and hydrophone (yellow cylinder) in between the accelerometers. The axes system define accelerometer orientation (a), DAVS Earth orientation and area bathymetry during BIOCOM'19 deployment (b).

shore rock made of basalt. The DAVS recorder was developed at CINTAL¹⁸ during the EU H2020 WiMUST project¹⁹ as a device for sensing acoustic particle velocity in Autonomous Underwater Vehicle-based seismic applications²⁰ and is covered by an international patent.²¹ Briefly, this device is composed of a 65 mm diameter-525 mm long Delrin tube with the recording electronics and a polyurethane sensing end with two tri-axial accelerometers (model 356A17, PCB Piezotronics) separated by an in-house built end-cupped cylindrical hydrophone of PZT piezoelectric material with the dimensions and axes orientation shown in Fig. 4(a). The setup of the recorder on Earth coordinates is important for a meaningful data analysis, so it was carefully deployed and axes orientation was recorded approximately as shown in Fig. 4(b): *x* axis pointing towards the sea surface, *z*-axis pointing to the rock wall, with accelerometer #50 towards the wall and #49 towards the bay, and *y* axis oriented approximately parallel to the rock wall. The possibilities of differential particle velocity field offered by the

two closely spaced tri-axial accelerometers were not used in this paper.

According to the manufacturer the accelerometers have a flat sensitivity of 0.051 V/m/s² (−25.84 dB/1 V/m/s²) in a frequency band from 1 Hz to 5 kHz. However, different values were measured after polyurethane encapsulation of the two accelerometers in DAVS, as shown in Fig. 5 for the *Y* axis. A spline fitting curve to a few calibration experimental points show a deviation of approximately 6 dB from the nominal value at 2 kHz and were used in the processing of the data of this work. The hydrophone was measured to have a flat sensitivity of −197 dB/1 V/μPa within the [0–5] kHz band. The DAVS acquisition system codes the seven data channels (three axes per accelerometer and one for the hydrophone) in 24 bit words using a multi-channel Sigma-Delta analog to digital converter and archives the data in loss-less WAV format. Because the acquisition system was adapted from an acoustic pressure channel system, all channels were high pass filtered at 50 Hz. The sampling frequency is 10 547 Hz. The DAVS is powered by an external Li-ion battery pack.

C. Biological sampling

For the benthic fauna census, the photo-quadrat method was used. The photos were taken using a digital camera coupled to a square PVC frame with 0.35 m side, totaling an area per photo of 0.16 m². Five vertical transects were carried out, the first in front of the recorder, and the remaining four at 5 and 10 m distance to each side of the first one. A photo was taken at each linear meter of the coast, as well as records of distance traveled and depth of the site. The images obtained were treated in Photoshop 7.0 and analyzed in the CPCe 4.1 program (Coral Point Count with Excel files). To estimate the percentage of organism coverage, a grid with 36 points uniformly distributed was superimposed on the images.

For snapping shrimp that live under rocks and cracks hidden for most of the day, the methodology to estimate the

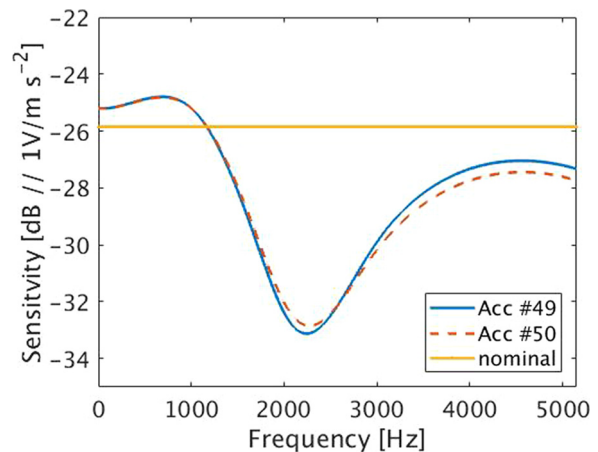


FIG. 5. (Color online) Accelerometer sensitivity frequency response along *Y* axis: #49 (thick-blue), #50 (dashed-red) and manufacturer nominal value (thick-yellow).

density was differentiated. An intensive search was carried out for 30 min at the interface between the rocky shore and the sand, at a maximum distance of 10 m with 0.5 m width. Also, covo-type traps were used, placed for a period of 12 h. In addition, an individual of each species was collected to allow identification in the laboratory.

D. Acoustic data analysis

Data analysis focus on the periods of the sea trial where the DAVS was active. Due to a shortage of battery modules for the required power consumption the DAVS was deployed and then recovered for battery charging and then redeployed. The data intervals are as follows (time is UTC):

- Day1: 10:19 January 14 to 10:05 January 15,
- Day2: 17:48 January 16 to 16:26 January 17,

which correspond approximately to 24h recording for each deployment. We will refer to those two periods as Day1 and Day2. Due to active acoustic transmissions performed during BIOCOCOM'19 only 75 s worth of ambient noise data were available approximately every 5 min, which required cross-correlation detection of active transmissions followed by data segmentation. It should be noted that local time in Rio de Janeiro is normally UTC-3 but in the austral Brazilian summertime, Day Saving Time (DST) is observed so, local time during the BIOCOCOM'19 experiment is actually UTC-2.

The DAVS records three types of data:

- (1) a set of attitude sensors for recording roll, pitch and heading,
- (2) acoustic pressure field in one hydrophone, named as P ,
- (3) acoustic particle acceleration field sensed along three perpendicular axes, named as A_x , A_y , and A_z , in two closely separate sensors, #49 and #50, one on each side of the hydrophone.

Attitude sensors' recording for Day1 and Day2 (not shown) confirm the orientation of Fig. 4(b).

Since acoustic pressure and particle acceleration were obtained from two different sensor types within the same enclosure, the first step taken in the processing was to compare their outputs for checking level coherence but also to detect possible differences along time and/or frequency. One way to perform this comparison is by reducing particle acceleration to equivalent acoustic pressure. The term "equivalent" is used here to differentiate acoustic pressure deduced from acceleration from that directly measured on the hydrophone.

The fundamental relation connecting equivalent acoustic pressure and particle velocity in the harmonic case and for plane waves is²²

$$v_p = zv, \tag{1}$$

where v_p is the equivalent acoustic pressure derived from scalar particle velocity v and z is the specific acoustic impedance. All terms in this equation are, in principle, complex. The plane wave regime applies for frequencies above the cut-off frequency given by²³

$$f_{\text{cut-off}} = \frac{c_w(\pi - \rho_s/\rho_w)}{2\pi H \sin[\arccos(c_w/c_s)]}, \tag{2}$$

where c_w , ρ_w and c_s , ρ_s are the water and sediment compressional velocities and densities, respectively, and H is the water depth. Using the sketch of Fig. 3(b) and the values of $H = 8$ m, $c_w = 1524$ m/s, $\rho_w = 1026$ Kg/m³ for water, and $c_s = 5300$ m/s and $\rho_s = 2700$ Kg/m³ characteristic for basalt,²⁴ gives $f_{\text{cut-off}} = 16$ Hz. Therefore, above the cut-off frequency the plane wave assumption is in principle verified in the far-field. In that case the impedance z in Eq. (1) takes the particularly simple form of $z = \rho c$, with ρ the density and c the sound speed. This means that z is real and v_p and v are in phase. In the acoustic sources' near-field the acoustic wave becomes spherical and the specific acoustic impedance z is no longer real, and becomes (see page 158 of Ref. 22)

$$z = \frac{j\omega\rho r}{1 + jkr} = \rho c \frac{\kappa r}{\sqrt{1 + \kappa^2 r^2}} e^{j\theta}, \tag{3}$$

where ω is the angular frequency, r is the range, and $\kappa = 2\pi/\lambda$ is the angular wavenumber with λ the wavelength. It can be seen that $\theta = \arctan(1/kr)$, the phase angle between v_p and v , varies from nearly 90° for small values of kr (near-field) to nearly 0 for large values of kr (far-field). In the near-field, the equivalent pressure wave amplitude is affected by the module ratio on the right hand side of Eq. (3). In order to illustrate this for the case at hand, Fig. 6 shows the specific acoustic impedance module ratio for a range $r = 7$ m (shortest straight line distance between the recorder and the rocky shore) as a function of frequency (a) and its effect on the calculation of the equivalent acoustic pressure with and without the spherical assumption, compared with directly measured acoustic pressure (b), as a function of frequency. For the experimental configuration used in BIOCOCOM'19, the spherical assumption only produces relevant effects for a frequency range below approximately 50 Hz. Particle acceleration derived acoustic pressure also tends to be significantly different from directly measured acoustic pressure at low frequency.

In the frequency domain, the equivalent of Eq. (1) in the far-field and above the cut-off frequency is given by

$$\begin{aligned} V_p(\omega) &= \rho c V(\omega) \\ &= \frac{\rho c}{j\omega} A(\omega) \\ &= \frac{\rho}{j\kappa} A(\omega), \end{aligned} \tag{4}$$

where $V_p(\omega)$ and $V(\omega)$ correspond to the frequency domain versions of v_p and v of Eq. (1), respectively, $A(\omega)$ is the acoustic particle acceleration field also in the frequency domain, and where all other terms have been previously defined. In practice, the measured accelerations are transformed to frequency domain using a fast Fourier transform and then Eq. (4) is used to get $V_p(\omega)$ for all the various acceleration channels (one along each axis). Note that

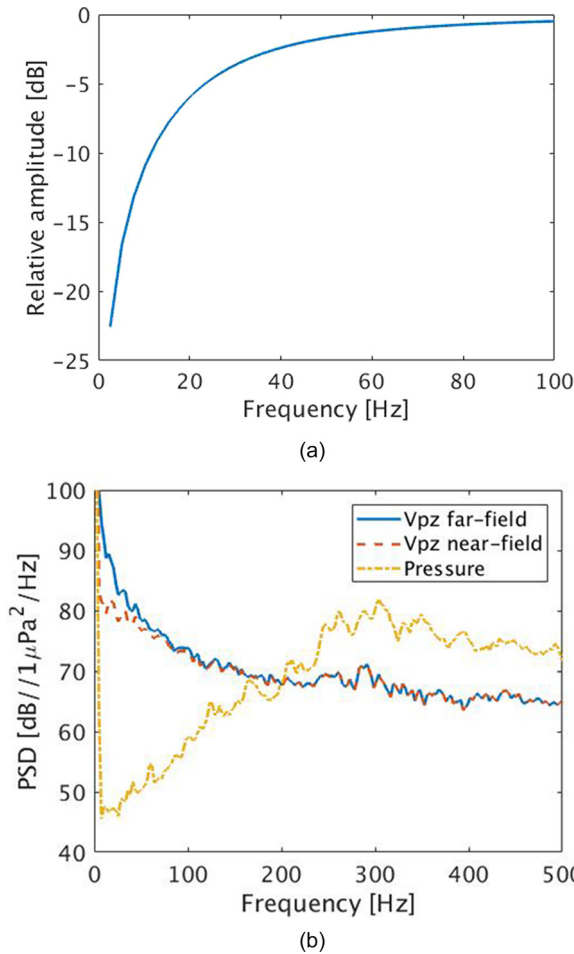


FIG. 6. (Color online) Illustration of the spherical wave effect in the near-field at 7 m range: the specific acoustic impedance module in the right hand side of Eq. (3) (a) and its comparison on the power spectral density of the z -component of particle velocity with the far-field (thick-blue) and near-field (dashed-red) assumptions, and for reference, the measured acoustic pressure (dash-dot-yellow) (b).

dividing by $j\omega$ from acceleration to velocity implies a low pass filter with a slope of -20 dB/decade showing an infinite gain at $\omega = 0$ and a gain of 1 (0 dB) at $\omega = \rho c$. This low-pass filter is somehow countered by the range dependent factor in Eq. (3) at short range.

In this case, sample power spectral density (PSD) and power spectrum will be estimated using the relations and normalization set out in Ref. 27.

Finally, a brief analysis of the directional content of the data is performed using the tri-axial vector sensor data using the method proposed in Ref. 20 for steering the cardioid formed by combining pressure and particle velocity equivalent pressure of accelerometer output through all elevation and bearing directions referred to the DAVS location. Thus, the steered azimuth θ and elevation ϕ acoustic pressure output at circular frequency ω is given by

$$\begin{aligned} \tilde{P}(\omega, \phi, \theta) = & P(\omega) + V_{px}(\omega) \sin(\phi) \\ & + V_{py}(\omega) \cos(\phi) \cos(\theta) \\ & + V_{pz}(\omega) \cos(\phi) \sin(\theta), \end{aligned} \quad (5)$$

where $P(\omega)$ is the hydrophone acoustic pressure field, $V_{px/y/z}$ are the pressure equivalent particle velocity fields for the respective axes x, y, z , and the angles are defined as azimuth $\theta \in [0, 2\pi]$ and elevation $\phi \in [-\pi/2, \pi/2]$ with zero azimuth aligned with axis y and positive elevation pointing to the surface.

Alternatively, assuming the planewave approximation and considering that the biological information of interest is uncorrelated and of much larger amplitude than the other ambient noise components (environmental and anthropogenic), one may obtain an estimate of azimuth as²⁵

$$\hat{\theta} = \arctan \frac{\langle p(t)v_{pz}(t) \rangle}{\langle p(t)v_{py}(t) \rangle} \approx \arctan \frac{\mathbf{u}_z}{\mathbf{u}_y}, \quad (6)$$

where $p(t)$ is the acoustic pressure, $v_{pz}(t)$ and $v_{py}(t)$ are the pressure equivalent particle velocity z and y sensor outputs, respectively, where $\langle \cdot \rangle$ represents time average and stands for an estimate of the zero-lag cross-correlation, and where \mathbf{u}_z and \mathbf{u}_y are unitary vectors along the respective axes. The previous relation also implicitly assumes that sensors along directions z and y have the same gain and that they are co-located with the pressure sensor.

III. RESULTS AND DISCUSSION

A. Biological assessment

The biological survey was performed on December 20, 2016 on the rocky shore of Cabo Frio Island, facing the DAVS recorder location. The coverage of invertebrate is abundant and rich with essentially four species distributed according to the tidal region. Table I shows the distribution of the (assumed) soniferous species, together with their emitting frequency bandwidth.²⁶ Since snapping shrimp are relatively difficult to visually spot, it is anticipated that the above referred count in the infratidal region may be largely underestimated, since the underwater recordings clearly show evidence of the characteristic snapping shrimp “cracking” noise attributed to the *Synalpheus parneomeris* family.²⁸ The right hand side column of Table I shows the estimated emitting bandwidth for each species which allows to set the overall band to approximately above, say, 1 kHz. Of course, the full spectrum is far more complex since other variables such as emitting power spectrum per species, abundance, tidal region, duration and spatial distribution interplay to form the actual chorus.

B. Acoustic data

1. Sound pressure and particle velocity

The BIOCOT’19 experiment took place during the austral summertime when there is significant boating and beach activity in the area. This activity leads to relatively loud anthropogenic sound sources, especially during the day time, roughly between 10:00 and 17:00 local time. Also, as explained above, active source transmissions were

TABLE I. Rocky shore species assessment Ref. 26.

Region	Species	Abundance (m ⁻²)	Band (kHz)
High intertidal	bivalves	2600	20–27 ^a
	barnacles	2700	1.5–25 ^b
Low intertidal	bivalves	10	20–27 ^a
	barnacles	4500	1.5–25 ^b
	sea urchins	2.8	0.8–2.8 ^c
Infratidal	sea urchins	5	0.8–2.8 ^c
	shrimp	2 ^d	2.5–20 ^e

^aReference 29.

^bReference 30.

^cReference 31.

^dPossibly underestimated.

^eReference 28.

performed for other experiment objectives, which involved significant boat movement in the vicinity of the recorder.

In order to obtain an overview of the PSD variation over time, percentiles are often used. A PSD percentile p is the spectral level below which the PSD lies $p\%$ of the time. These are shown in Fig. 7 for the hydrophone recordings of Day1. The noise due to boating activity can be clearly seen in the band below 1 kHz, peaking at 200 Hz in the 75 and specially 95 percentiles, reaching a PSD level above 80 dB// 1 $\mu\text{Pa}^2/\text{Hz}$. The difference between percentile 5, believed to be achieved during the night period, and percentile 95 reached around noon, is approximately 35 dB at 200 Hz, which compares with values found in Ref. 17. Although this statistic covers only one day, it is clear that there are two bands arbitrarily separated at approximately 1.5 kHz: the band below that frequency, prone to highly energetic anthropogenic noise during day time, and the band above, rich of environmental (wind, waves) and biological components, according to the biological assessment of Sec. III A. So, the analysis will focus in two bands: the so-called “biological band” above 1.5 kHz aiming at determining whether the biological chorus from the rocky shore can be heard and the

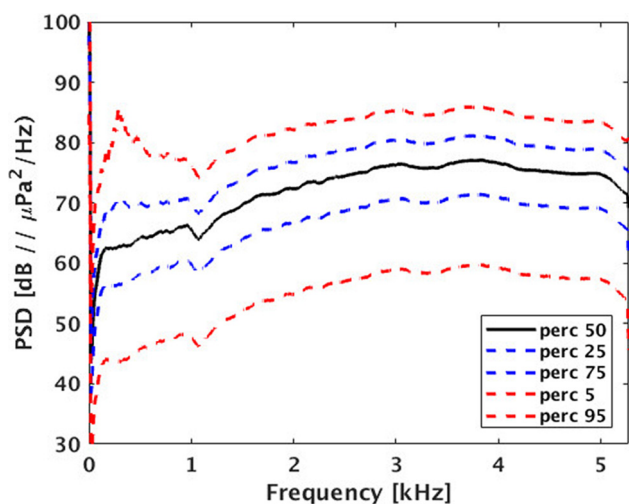


FIG. 7. (Color online) Acoustic pressure PSD percentiles for Day1 obtained from hydrophone recordings.

low band, roughly below 500 Hz, where the particle motion field differentiates from the acoustic pressure field at close range and near boundary surfaces.

The PSD estimates of the 75 s long snapshots recorded every 5 min throughout Day1 are shown in Fig. 8 for the frequency band above 1.5 kHz. Plots (a)–(c) show the pressure equivalent particle velocity for the two accelerometers axes x - z , respectively, while plot (d) shows the corresponding PSD estimate for the hydrophone measured acoustic pressure. Comparing plots (a)–(c) to (d), the following comments can be made.

- (1) It is comforting to see that acoustic pressure and the pressure equivalent particle velocity calculated from accelerometer data show an overall agreement PSD level between 70 and 80 dB, throughout the nearly 200 traces acquired during the period of 24 h.
- (2) The component V_{px} in accelerometer #49 (bay side) has a larger amplitude than in accelerometer #50 (rocky shore side) while the z component (pointing to the rocky shore) shows exactly the opposite, and this difference increases with frequency, being more pronounced above 3 kHz, denoting an increasing activity towards the rocky shore.
- (3) y axis components (parallel to the shore) show the same PSD for both accelerometers.

By summing the received noise PSD for each available 75 s period over the recording day, for the frequency band above 1.5 kHz one gets the total received energy along time, as shown in Fig. 9 for Day1. The pressure channel in plot (d) clearly shows the dawn-dusk chorus pattern with a substantial signal power increase and a parallel decrease during the night period up to 2 dB down compared with the mean day level. This pattern is clearly reflected in the particle velocity channels with, however, a number of spurious peaks of larger relative energy, more frequent in the x and y axes. Since those axes are those pointing to the surface and along the shore to the Boqueirão strait, through which there is frequent movement of touristic and fishing boats during the day and night, respectively, these power peaks are most probably associated with anthropogenic noise sources. The z -axis, the one pointing towards the rocky shore, shows the most clearer pattern with the higher signal level and where accelerometer #50 (the one towards the rock) shows a level that is approximately 4 dB higher than that of accelerometer #49 (to the open bay side). This behavior is changed in the other axes since for the y axis the two accelerometers have approximately the same level, and for the x axis the behavior is reversed: accelerometer #49 has a large amplitude than #50.

2. Field directionality

The next step is to extract directional information for the 75 s snapshots recorded during Day1. The various ways to do this are discussed in Sec. II. Figures 10 and 11 show estimated azimuth and elevation along time during Day1, using Eqs. (5) and (6), respectively. For Fig. 10, each

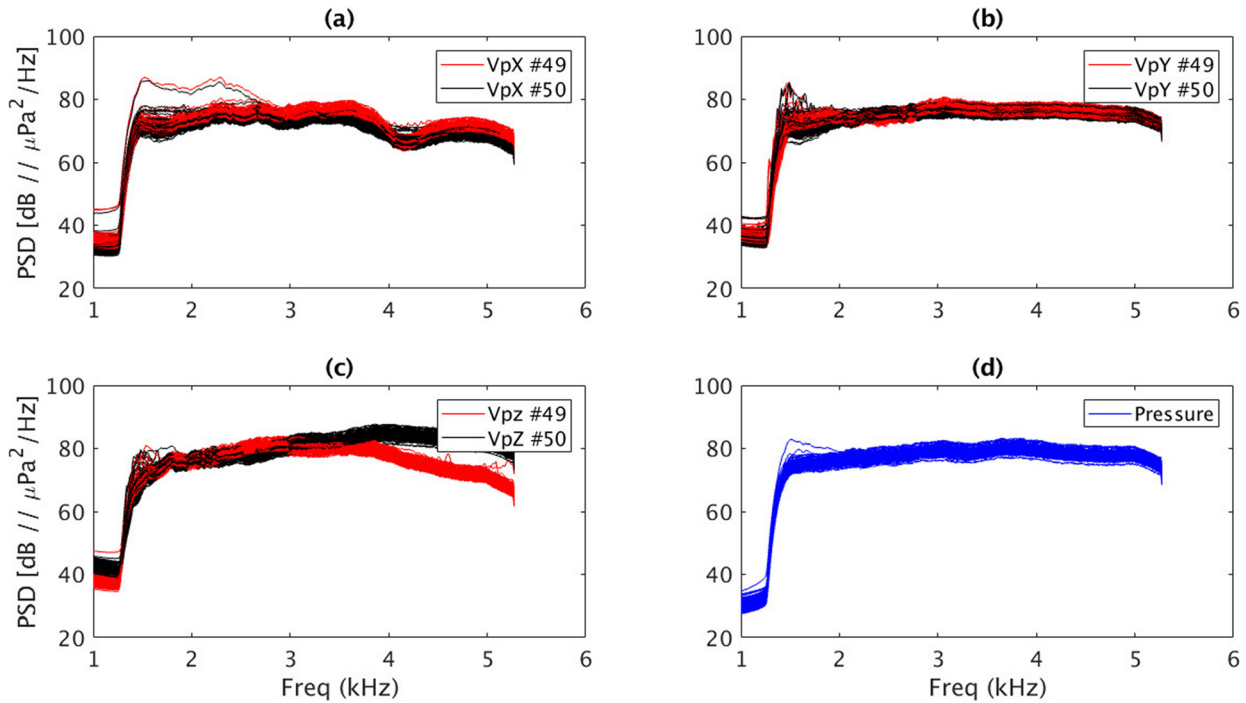


FIG. 8. (Color online) PSD noise spectra estimates, each line corresponds to 75 s of data taken approximately every 5 min during Day1 (January 14–15) for the frequency band above 1.5 kHz; pressure equivalent particle velocity for x axis (a), y axis (b), z -axis (c), and hydrophone measured acoustic pressure (d). Accelerometer #49 in red and #50 in black in plots (a)–(c).

estimate was obtained by 1.5 kHz high-pass finite impulse response filtering each channel, then transformed into the frequency domain and time averaged through the 75 s noise window. Channels are then combined using Eq. (5) and the resulting $\bar{P}(\omega, \theta, \phi)$ is averaged over the frequency band. The resulting surface is searched for the absolute maximum

in the full $[0^\circ, 360^\circ]$ for azimuth and $[-90^\circ, 90^\circ]$ for elevation. Instead Fig. 11 is obtained by time cross-correlating the 1.5 kHz high-pass filtered equivalent pressure v_{pz} and v_{py} with acoustic pressure p , over each 75 s window, and the estimated azimuth plotted through time. The results for Day1 show that bearing estimates coincide at around 80° ,

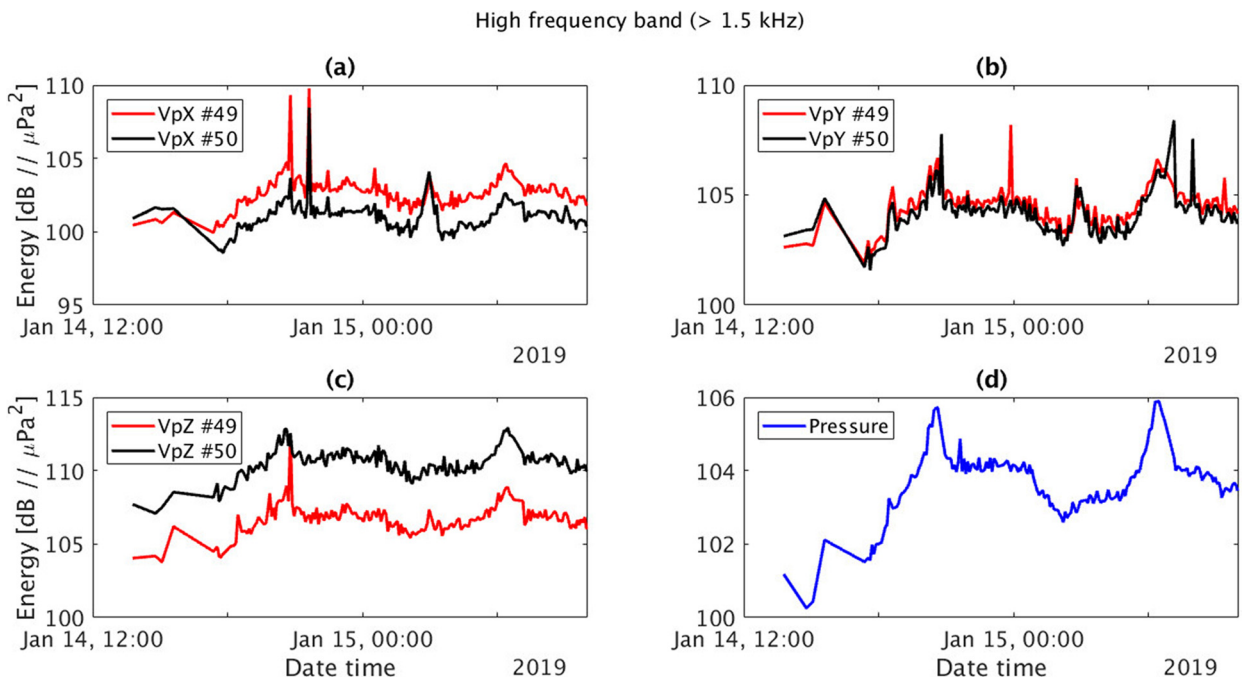


FIG. 9. (Color online) Sum of received PSD on the DAVS channels for Day1 (January 14–15) in the frequency band above 1.5 kHz; pressure equivalent particle velocity for x (a), y (b), z -axes (c), and acoustic pressure (d). Accelerometer #49 in red and #50 in black in plots (a)–(c).

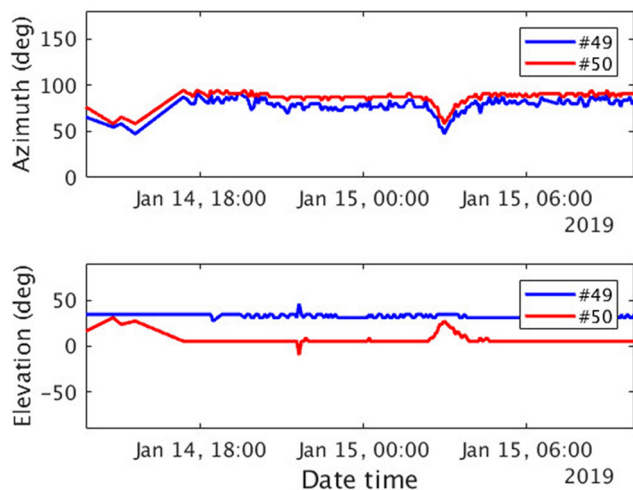


FIG. 10. (Color online) Day 1 (January 14–15) bearing and elevation estimates for accelerometers #49 and #50 using Eq. (5).

thus pointing to the rocky shore, for both accelerometers, with an estimate through time that is slightly more noisy for #49, the accelerometer on the bay side, than for accelerometer #50, the one on the rocky shore side. Elevation is estimated approximately 25° – 30° for #49 and around 0° (horizontal) for #50. This difference is probably due to the fact that #50 is directed towards the direct path of biological noise generated on the rock, while #49 is directed towards a surface reflection of it, also because it is shadowed by #50.

3. Particle acceleration

Figure 12 shows a 20 s time series snapshot of acceleration data taken on Day 1 after dark, where a disturbance generates a quick succession of acceleration impulses on the x and y axes. The difference between accelerometers #49 and #50, much clearer and stronger in #49 than in #50, make us hypothesize that the disturbance source is passing above and on the bay side of the recorder location. Slight offsets of a

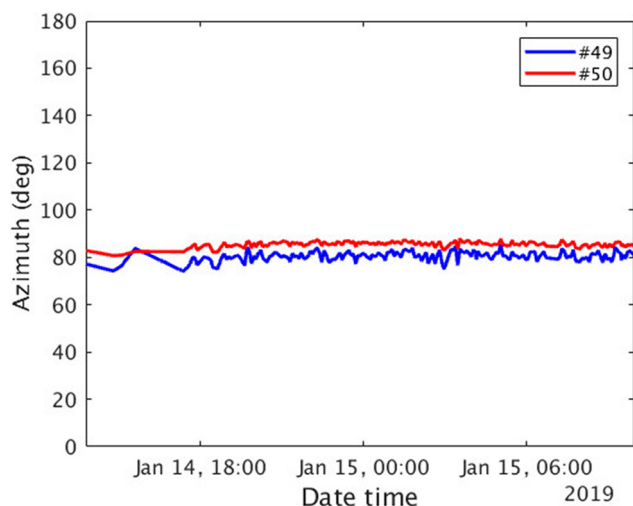


FIG. 11. (Color online) Day 1 (January 14–15) azimuth estimates using cross-correlation (6).

few mm/m/s^2 , variable from channel to channel, can be noted in all channels. Figure 13 shows the mean PSD of the acceleration and pressure channels, calculated through the Welch method (also known as periodogram) in the 75 s intervals recorded for Day 1 (January 14–15) and over the low frequency band 0–500 Hz. First, a Welch PSD is obtained for each 75 s interval using a sliding block size of 4096 samples, corresponding to approximately 0.5 s, with a 50% overlap between data segments. Second, an average of the PSDs over 12 consecutive intervals is performed with again a 50% overlap of six intervals. The PSD is shown for the three x , y , and z axes and for the two accelerometers #49 (left) and #50 (right). The acoustic pressure measured Prs in the hydrophone channel is also shown for reference (bottom left). One can remark a significant sound pressure (plot Prs , bottom left) increase up to 90 dB, in the band above 150 Hz, peaking at 300 Hz until 22:00 UTC, i.e., 20:00 local time. The same levels seem to be picking up again in early morning at 09:00 UTC (07:00 local) on January 15. The acceleration data shows its highest levels for low frequencies below 100 Hz, apart from a solitary peak at 400 Hz in the x axis (pointing upward). There are strong time-frequency coincident peaks in the y and z axis at around 19:00 UTC (17:00 local) on the 14th and then at 09:00 UTC on January 15th. Recall that y and z point along and towards the rocky shore, respectively. There is also a consistent night time spread increase of acceleration power spectral density close to or below 50 Hz in accelerometer #50, the one facing the rock and this is particularly relevant in the z axis, pointing towards the rocky shore.

C. Discussion

According to the official bulletin of the Brazilian National Observatory for year 2019, in the region of Cabo Frio (RJ), sunset would occur at 19:40 on January 14 and sunrise at 6:16 on January 15 (UTC-2), which approximately coincides with the timing of the maxima of Fig. 9(d), with a dusk and dawn duration of approximately 1 h to 1 h 30 min. After sunset, the received sound pressure remained approximately stable for about 3 to 4 h and then decreased to a minimum during the morning at around 3 am, then slowly raised up to the dawn chorus maximum power. The same pattern is observed in the particle velocity directional channels with a high number of interferences of unknown origin. Differences in received power in the two accelerometers seem to be attributed to shadowing for biological noise coming from the rocky shore or, vice versa, for noise coming from the bay side. The combination of these channels for estimating noise directionality along the recording time period and for the band >1.5 kHz clearly show that the predominant sound level always arises from the rocky shore side, as shown in Figs. 10 and 11. However, analyzing a typical azimuth - elevation surface as that shown in Fig. 14 for the morning of January 15, one can see a secondary strong peak pointing towards the bay. This secondary peak has higher amplitude during the day time and changes position,

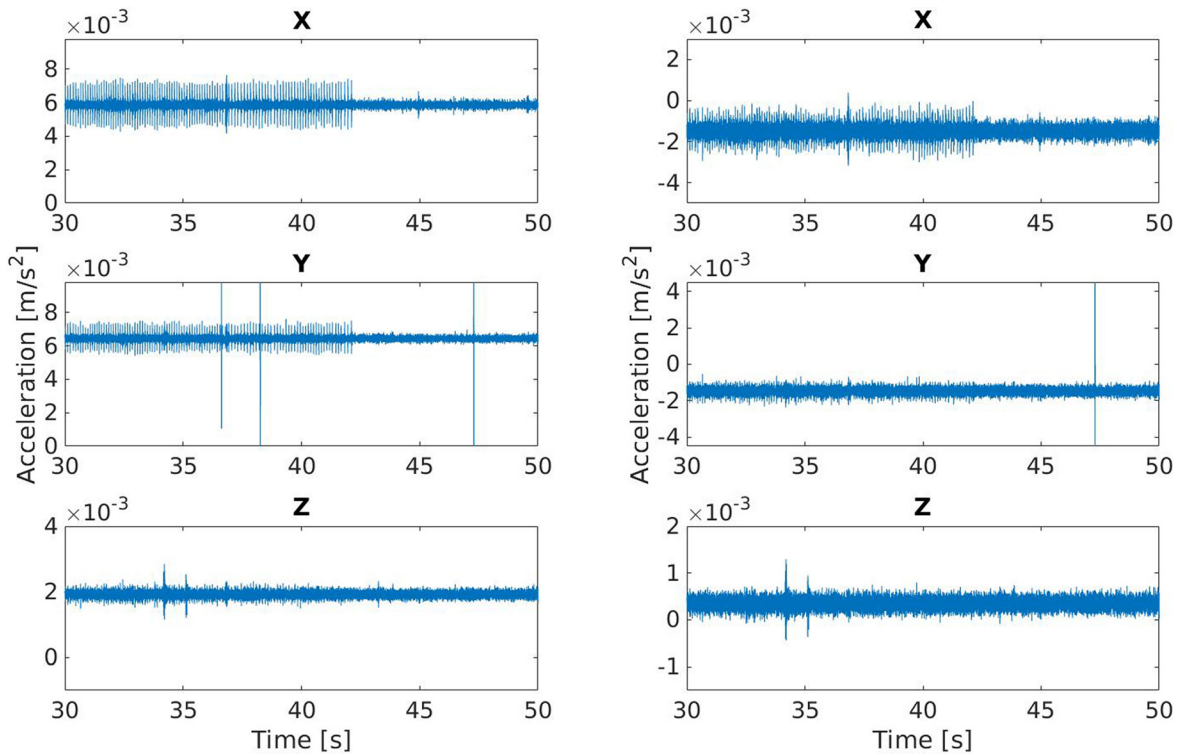


FIG. 12. (Color online) Received particle acceleration 20 s snapshot after dark of Day1 (January 14–15): the three directional channels x , y and z for accelerometers #49 (left) and #50 (right).

so it is believed to be associated with noise sources due to boating in the bay side. The angular resolution is low, so it is difficult to associate this peak to any particular known source. It is possible that, at moments, it corresponds to more than one source for a distance varying from a few hundred meters up to 3 km. Nevertheless, this confirms that the sound pressure received above 1.5 kHz is predominant in the

area and is of biological origin generated in the rock facing the recorder. The acceleration data in the low frequency band <500 Hz of Fig. 13 shows a quite different pattern: maxima are located well before dusk and dawn; these maxima are time aligned in channels y and z (for both accelerometers) and below 250 Hz; time coincident maxima also appear in the x axis but clearly above 350 Hz. The particle

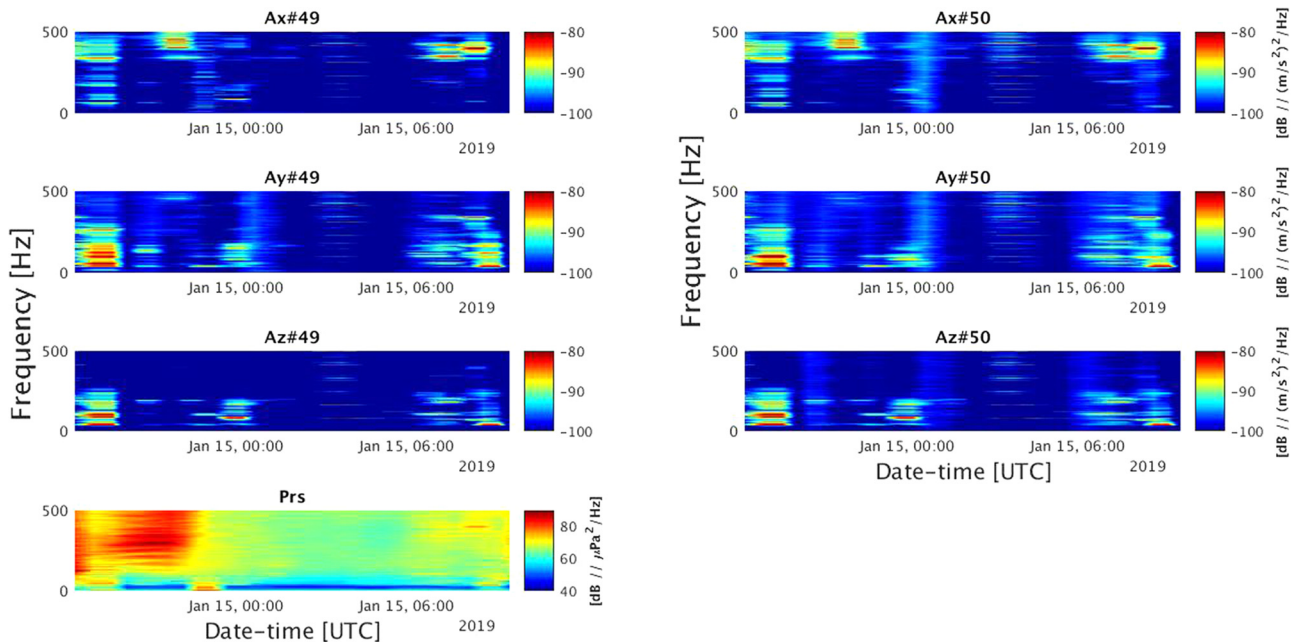


FIG. 13. (Color online) PSD of received particle acceleration and pressure for Day1 (January 14–15): the three directional channels x , y , and z for accelerometers #49 (left) and #50 (right). Hydrophone pressure channel is shown for reference (bottom left).

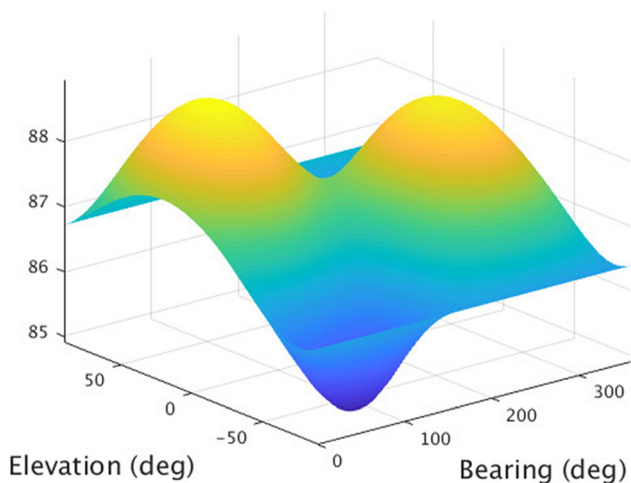


FIG. 14. (Color online) Day1 (January 14–15) bearing-elevation surface in the morning of January 15th, using data from accelerometer #49.

acceleration field generated in the rock wall before dusk is clearer by inspecting a time zoom of the period between 18:30 and 21:00 UTC (16:30–19:00 local) of January 14, as shown in Fig. 15. Time resolution is low which smears the figure, but it can be seen that particle acceleration is concentrated below 120 Hz, with different components in y and z axes. Whether that increase of particle acceleration may be associated with water agitation or any other activity coming marine life in the rocky shore is unknown.

IV. CONCLUSIONS

During the BIOCUM'19 sea trial, a vector sensor hydrophone was deployed for two periods of one day near a marine life rich rocky shore in the bay of the Cabo Frio

island, Rio de Janeiro, Brazil. Since the two days show similar results, the analysis focuses on the first day, January 14–15, 2019. The lessons learned may be summarized as follows: from an experimental point of view, the vector sensor hydrophone allows for measuring both acoustic pressure and particle acceleration, and derives the acoustic field directionality in a single, robust and easy to deploy compact recorder; care must be taken during experiment design and deployment, such that distances from surface or bottom allow for a cut-off frequency well below the frequency band of interest and that the far-field assumption holds; also, the recorder must be fixed and its position and orientation known at all times. For the Cabo Frio data set in particular, the analysis of the received data shows that a frequency of roughly 1.5 kHz separates two bands: the low frequency band where anthropogenic noise is predominant during day time with biological noise during dark hours, and the high frequency band where biological noise dominates at all times. The directional field calculated from the vector sensor indicates that the biological chorus from the rocky shore dominates the acoustic spectra. Furthermore, particle acceleration records show a low-frequency spectra (below 120 Hz) that peaks in the periods just before dawn-dusk, which may be associated with marine life activity in preparation for chorus. These results are validated by the biological assessment of the species distribution performed *in situ*. Further analysis of the directional data scanning through the rock wall may be able to determine sound patches variation throughout the day. In general, it can be said that rocky shore invertebrate noise is clearly audible throughout the day in the band above 1.5 kHz. The vector sensor hydrophone helps in discriminating biological noise when interference is present and allows for recording particle

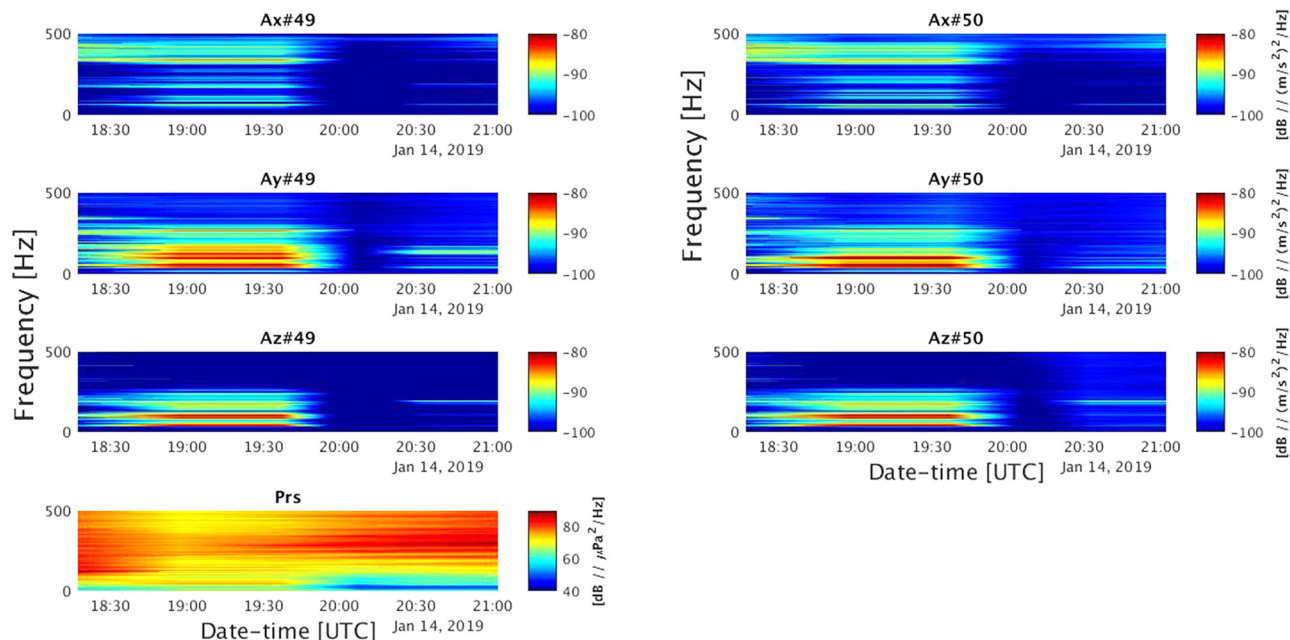


FIG. 15. (Color online) Estimated PSD for sunset period of January 14: channels x , y , and z for accelerometer #49 (left) and #50 (right); acoustic pressure is shown for reference (bottom left).

acceleration, adding information to the acoustic field in the low frequency band.

ACKNOWLEDGMENTS

The authors are grateful to the “Ciência sem Fronteiras” program (Brazil) for funding obtained through project BIOCUM (CNPq Contract No. 401407/2014-4) and for the support of the crew of the *Anchova* and IEAPM personnel during the BIOCUM’19 experiment. They are also grateful for funding from the FCT under the SEAFOX project (Contract No. PTDC/EEI-PRO/2598/2014), Portugal. Comments and discussions with P. Felisberto are greatly appreciated.

¹M. C. Hastings, “Coming to terms on the effects of ocean noise on marine mammals,” *Acoust. Today* **4**(2), 22–33 (2008).
²A. D. Hawkins and A. N. Popper, “Assessing the impact of underwater sounds on fishes and other forms of marine life,” *Acoust. Today* **10**(2), 30–41 (2014).
³S. E. Freeman, F. L. Rohwer, G. L. D’Spain, A. M. Friedlander, A. K. Gregg, S. A. Sandin, and M. J. Buckingham, “The origins of ambient biological sound from coral reef ecosystems in the Line Islands archipelago,” *J. Acoust. Soc. Am.* **135**(4), 1775–1788 (2014).
⁴M. B. Kaplan and T. Aran Mooney, “Coral reef soundscapes may not be detectable far from the reef,” *Sci. Rep.* **6**, 31862 (2016).
⁵R. Fay and A. N. Popper, *Comparative Hearing: Fish and Amphibians* (Springer, New York, 1990).
⁶L. Coquereau, J. Grall, J. Clavier, A. Jolivet, and L. Chauvaud, “Acoustic behaviours of large crustaceans in NE Atlantic coastal habitats,” *Aquat. Biol.* **25**, 151–163 (2016).
⁷L. E. Wysocki, A. Codarin, F. Ladich, and M. Picciulin, “Sound pressure and particle velocity acceleration audiograms in three marine fish species from the Adriatic Sea,” *J. Acoust. Soc. Am.* **126**(4), 2100–2107 (2009).
⁸A. N. Popper and A. D. Hawkins, “The importance of particle motion to fishes and invertebrates,” *J. Acoust. Soc. Am.* **143**(1), 470–488 (2018).
⁹A. Banner, “Measurements of the particle velocity and pressure of the ambient noise in a shallow bay,” *J. Acoust. Soc. Am.* **44**(6), 1741–1742 (1968).
¹⁰G. R. Potty, M. Tazawa, J. Giard, J. H. Miller, Y.-T. Lin, A. Newhall, and K. J. Vigness-Raposa, “Measurements of particle motion near the seafloor during construction and operation of the Block Island Wind Farm,” *J. Acoust. Soc. Am.* **141**, 3993 (2017).
¹¹P. Sigray and M. Andersson, “Particle motion measured at an operational wind turbine in relation to hearing sensitivity in fish,” *J. Acoust. Soc. Am.* **130**(1), 200–207 (2011).
¹²M. Lugli and M. L. Fine, “Stream ambient noise, spectrum and propagation of sounds in the goby *Padogobius martensii*: Sound pressure and particle velocity,” *J. Acoust. Soc. Am.* **122**(5), 2881–2892 (2007).
¹³C. E. L. Ferreira, J. E. A. Gonçalves, and R. Coutinho, “Community structure of fishes and habitat complexity on a tropical rocky shore,” *Environ. Biol. Fishes* **61**, 353–369 (2001).

¹⁴V. J. Giglio, M. L. F. Ternes, M. C. Barbosa, C. A. M. M. Cordeiro, S. R. Floeter, and C. E. L. Ferreira, “Reef fish associations with sea urchins in an Atlantic oceanic island,” *Marine Biodiversity* **48**, 1833–1839 (2018).
¹⁵L. Calado, A. Gangopadhyay, and I. C. A. da Silveira, “Feature-oriented regional modeling and simulations (FORMS) for the western South Atlantic: Southeastern Brazil region,” *Ocean Modell.* **25**, 48–64 (2008).
¹⁶F. B. Louza, J. Osowsky, F. C. Xavier, E. E. Vale, R. P. Vio, M. V. S. Simões, V. Barroso, and S. M. Jesus, “Communications and biological monitoring experiment in an upwelling environment at Cabo Frio island bay,” in *Proceedings of IEEE/MTS Oceans*, Marseille, France (June, 2019).
¹⁷D. Campbell, F. C. Xavier, U. G. Melo Junior, N. G. Silveira, L. V. Versiani, and E. B. F. Netto, “Underwater soundscape pattern during high season of nautical tourism in Cabo Frio island, Brazil,” in *Proceedings of the 5th International Conference on the Effects of Noise on Aquatic Life, POMA*, Den Haag, The Netherlands (July 2019).
¹⁸A. Mantouka, P. Felisberto, P. Santos, F. Zabel, M. Saleiro, S. M. Jesus, and L. Sebastião, “Development and testing of a dual accelerometer vector sensor for AUV acoustic surveys,” *Sensors (MDPI AG)* **17**(6), 1328 (2017).
¹⁹Funded under Contract No. ICT-645141 of the European Union under Horizon 2020 research program between 2015 and 2018.
²⁰P. Felisberto, P. Santos, and S. M. Jesus, “Acoustic pressure and particle velocity for spatial filtering of bottom arrivals,” *IEEE J. Ocean. Eng.* **44**(1), 179–192 (2019).
²¹S. M. Jesus and P. Felisberto, Patent No. PCT/IB2018/052167, WIPO (April 2018).
²²L. E. Kinsler, *Fundamentals of Acoustics*, 4th ed. (Wiley, New York, 2000).
²³S. L. Nedelec, J. Campbell, A. N. Radford, S. D. Simpson, and N. D. Merchant, “Particle motion: The missing link in underwater acoustic ecology,” *Meth. Ecol. Evol.* **7**, 836–842 (2016).
²⁴E. L. Hamilton, “Geoacoustic modeling of the sea floor,” *J. Acoust. Soc. Am.* **68**, 1313–1340 (1980).
²⁵P. Felisberto, J. Schneiderwind, P. Santos, O. Rodriguez, and S. M. Jesus, “Comparing the resolution of Bartlett and MVDR processors for bottom parameter estimation using pressure and vector sensor short array data,” in *Proceedings of Oceans–Bergen, 2013*, MTS/IEEE, Bergen, Norway (June 2013).
²⁶A. Kassuga (private communication, 2018).
²⁷S. M. Jesus, “Standards for power spectrum estimation: Matlab issues for acoustic pressure and particle motion,” CINTAL Report No. 03/19, University of Algarve (August 2019).
²⁸W. W. L. Au and K. Banks, “The acoustics of the snapping shrimp *Synalpheus parneomeris* in Kaneohe Bay,” *J. Acoust. Soc. Am.* **103**(1), 41–47 (1998).
²⁹L. Di Iorio, C. Gervaise, V. Jaud, A. A. Robson, and L. Chauvaud, “Hydrophone detects cracking sounds: Non-intrusive monitoring of bivalve movement,” *J. Exp. Marine Biol. Ecol.* **432–433**, 9–16 (2012).
³⁰BIOCUM technical report, IEAPM (2017).
³¹C. Radford, A. Jeffs, C. Tindle, and J. C. Montgomery, “Resonating sea urchin skeletons create coastal choruses,” *Marine Ecol. Prog. Ser.* **362**, 37–43 (2008).